Pacific Northwest National Laboratory

Physical Modeling of Spinel Crystals Settling at Low Reynolds Numbers

Micah J. Schaible
Montana Tech University
Office of Science, Science Undergraduate Laboratory Internship Program
Pacific Northwest National Laboratory
Correspondence: realcomfy@hotmail.com

Josef Matyas
Senior Scientist, Energy and Environment Directorate
Pacific Northwest National Laboratory
Richland, Washington

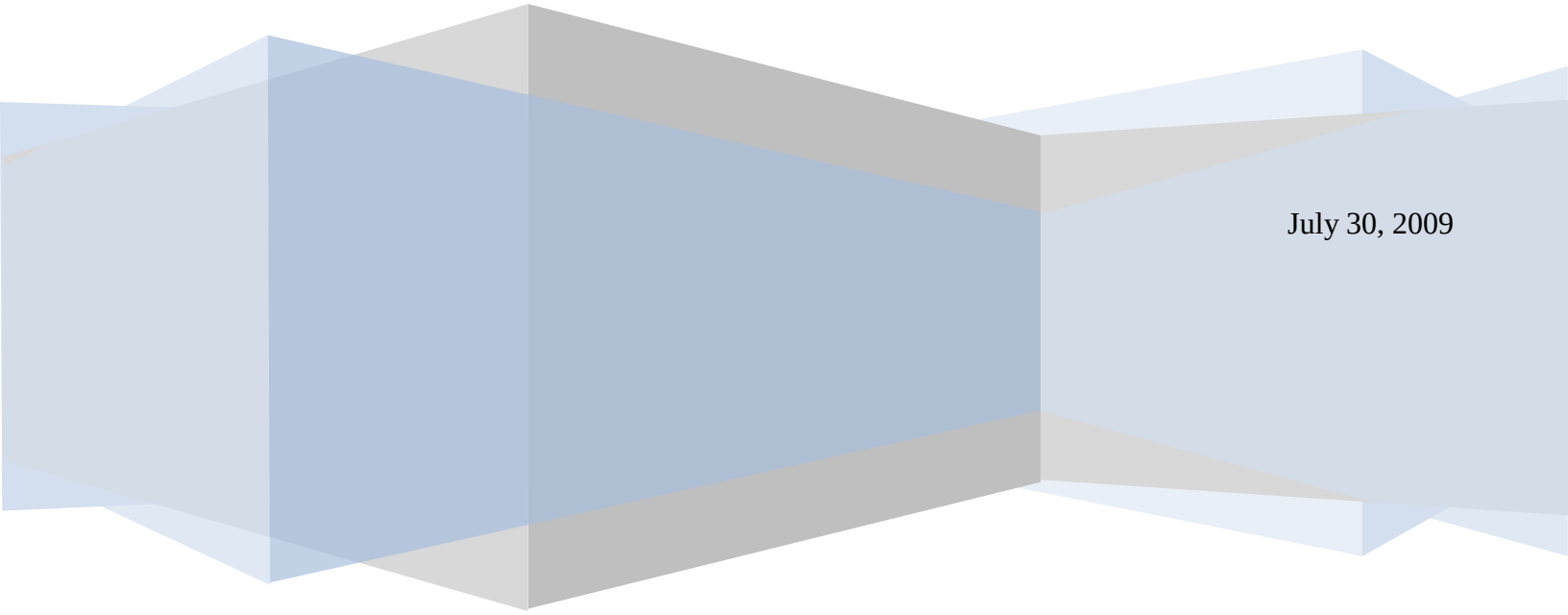

July 30, 2009

Table of Contents

List of Figures and Tables

Abstract

Physical Modeling of Spinel Crystals Settling at Low Reynolds Numbers.
Micah J. Schaible (Montana Tech University, Butte, MT 59701), Josef Matyas (Pacific Northwest National Laboratory, Richland, WA 99354)

The crystallization of large octahedral crystals of spinel during the high-level waste (HLW) vitrification process poses a potential danger to electrically heated ceramic melters. Large spinel crystals rapidly settle under gravitational attraction and accumulate in a thick sludge layer that may partially or completely block the glass discharge riser of the melter. The settling of single particles of different sizes and the motion of hindered settling front of different particle volume fraction suspensions were studied in stagnant, transparent-silicone oils at room temperature to help predict the settling behavior of spinel crystals in the riser. The dimensions and terminal settling velocities of single particles were measured using an optical particle-dynamics-analyzer. The data yielded an experimental shape factor for glass beads that differed only 0.73% compared to the theoretical shape factor for a perfect sphere. The experimental shape factor for the spinel crystals was smaller than that of the beads given the larger drag force caused by the larger surface area to volume ratio of the octahedral crystals, but matched the theoretically predicted value to within 10%. In the hindered settling experiments, both the glass bead and spinel suspensions were found to follow the predictions of the Richardson-Zaki equation with higher particle volume fractions settling at a slower rate. Particle concentration profiles obtained from color threshold analysis (CTA) indicated that for a given volume fraction the rate of clarification increases with an increase in settling vessel angle with respect to the vertical as predicted by the Ponder, Nakamura and Kuroda (PNK) model. The Stokes', Richardson-Zaki and PNK equations can adequately predict the accumulation rate of spinel crystals in the vertical or inclined glass discharge riser of HLW melters.

1. Introduction

The high-level radioactive waste (HLW) from the Hanford and Savanna River sites is being vitrified as a means of stable long term storage. A major concern of the vitrification process is the formation and settling of spinel crystals in the glass discharge riser of the HLW melter [1], [2]. During melter idling periods, while new feed is being incorporated into the melt, the molten glass in the riser is at approximately 850°C. At this temperature, a significant volume of large octahedral crystals of spinel $[Fe,Ni,Mn,Zn][Fe,Cr]_2O_4$ can form [8]-[10]. These crystals rapidly settle into a thick sludge layer that may partially or completely block the glass discharge riser.

The main factors that control the accumulation rate of spinel crystals in the melter are: 1) the size of crystals, 2) the extent of crystal agglomeration, and 3) hindered settling effects [2]. Under melter idling conditions, where the particle Reynolds numbers (*Re*) of spinel crystals are on the order of 10^{-6}, the dominating factor controlling the terminal settling velocity is the effective size of the crystals. At these low *Re*, the Stokes' equation for spherical particles can be used to predict terminal settling velocity to within 1% [3]:

$$u = \frac{2(\rho_p - \rho_f)gr^2}{9\mu} \qquad (1)$$

where ρ_p is the particle density, ρ_f is the fluid density, μ the dynamic viscosity, g the gravitational acceleration and r the particle radius. The factor 2/9 is calculated by assuming a perfect sphere settling at a constant rate in a quiescent fluid with a balance between the downward gravitational force and upward buoyancy and drag forces. For non-spherical particles, the Stokes shape factor k can be calculated from:

$$k = \frac{u'}{u} = \frac{2}{9}\frac{u'\mu}{(\rho_p - \rho_f)gr_v^2} \qquad (2)$$

where u' is the experimentally measured terminal settling velocity of the non-spherical particle and r_v is the effective radius. Thus, if the density and viscosity of the fluid and the size and density of the particle are known, the shape factor can be calculated from experimentally measured terminal settling velocities. A review of the various methods to calculate the drag on non-spherical particles was performed by Chhabra et al. [5] and a more recent study concentrating on isometric particles, including octahedrons, was undertaken by Hazzab et al. [6].

In particle volume concentrations as low as 1%, hindered settling effects such as particle-particle interactions and upward flow due to fluid displacement as particles travel downwards cause a noticeable slowing in the settling velocity [7]. One of the most widely used empirical relationships to calculate the hindered settling velocity u'' of a suspension of uniformly sized spherical particles is the Richardson-Zaki equation:

$$u'' = u(1 - C_0)^n \qquad (3)$$

where C_0 is the initial particle concentration in the mixture and n is an exponent which for $R_e \leq 0.2$ is approximately equal to 4.65 [3]. In polydisperse suspensions, the relative motion between particles causes distinct regions of varying concentration to form [7]. This and other dispersive effects cause a broadening of the zone between the region of original concentration and clarified fluid [11].

Another phenomenon of importance for a complete understanding of spinel settling in the melter spout riser is an increase in volumetric settling rates for suspensions settling in inclined vessels [7], [13]. This effect can be explained by an increase in surface area onto which the particles can settle. The rate at which the volume of clarified fluid increases, including the thin

strip that forms along the downward facing wall, can be explained by the Ponder, Nakamura and Kuroda (PNK) model:

$$S(t) = u''b\left(\cos\varphi + \frac{L}{b}\sin\varphi\right) \quad (4)$$

where φ is the angle of inclination measured with respect to the vertical, L is the total length of the settling vessel, and b is the vessel width. This equation shows that the rate at which the suspension clarifies increases up to a maximum for a vessel horizontal to the surface it is resting on.

Williams et al. reviewed a number of different techniques commonly employed to study sedimentation such as x-ray attenuation and NMR imaging [12]. However, optical monitoring was used in this study because it allowed direct observation of settling particles and fast evaluation of collected data. To improve predictions of the accumulation rate of spinel crystals in the glass discharge riser during melter idling, the settling of single particles of different sizes and the motion of the settling front for different volume fractions of particles in stagnant transparent liquids at room temperature were studied with an optical particle-dynamics-analyzer.

2. Materials and Methods

i. Material Acquisition and Composition

Settling experiments were performed with spherical barium calcium silicate glass beads and octahedral spinel crystals. The particles were suspended in Brookfield 5,000 cP standard viscosity oil of specific gravity 0.97. The glass beads were supplied in several size ranges by Mo-Sci Corporation and had a density of 4.1741 g/cm^3 (as-measured with gas pycnometer). The spinel was obtained from a waste simulant glass that was heat-treated at 850ºC for 10 days, allowing the spinel crystals to nucleate and grow to the desired size. After cooling, the glass was

broken into small pieces and dissolved in a heated solution of 25% nitric acid to obtain a mixture of spinel crystals and silica gel. The mixture was then treated with diluted hydrofluoric acid to dissolve the gel and the pure crystals were separated into distinct size groups with sieving. Crystals composition of was determined with SEM-EDS (scanning electron microscopy and energy dispersive spectroscopy) analysis. The crystals contained about 31.4 mass % of Ni, 48.3 mass % of Fe, 1.3 mass % of Cr, and 19 mass% of O. In addition, the density of the spinel crystals, 5.3954 g/cm^3, was obtained with a gas pycnometer. Figure 1 shows the SEM images of small and large glass beads and the isolated spinel crystals.

ii. Free Settling

To study free settling of individual glass beads and spinel crystals, a small amount of particles were sprinkled through a sieve into a 2.5x2.5x15cm clear quartz cuvette filled with silicon oil. The cuvette was tall enough for particles to reach their terminal settling velocity while the width was large enough that the wall effect on free-settling rates could be neglected. An infinitely corrected 20x/0.42 lens connected to a digital camera was focused at the center of the cuvette approximately 4 cm above the bottom (well below the region where particles reached their terminal settling velocities). PAX-it imaging software was used to record images at 5 second intervals and the size and vertical position of the particles were measured using dimensional analysis tools. The velocity was calculated by dividing the difference in distance between successive images by the known time interval. The experimental setup is shown in Figure 2.

Since the viscosity and density terms in (1) were known, a unique shape factor for each imaged particle was calculated from the measured sizes and velocities. While the effective radius of the glass beads was measured directly from collected images, the non-spherical shape of the

spinel crystals required the radius of an equivalent volume sphere to be calculated. To do this, the average length of the crystal edge (*a)* was measured and the volume of an isometric octahedron calculated from the equation $V_s = \frac{1}{3}\sqrt{2}a^3$. Then, the equivalent radius was obtained from the equation $r_{eq} = \left(\frac{3V_s}{4\pi}\right)^{1/3}$. Figure 3 details identification of crystal edge length from the shallow three-dimensional images.

In the case of agglomerates, an equivalent volume sphere could not be calculated because the crystals overlapped, making it impossible to accurately determine the volume. As a result, an area equivalent radius was determined from the measured boundary area of the agglomerates A_{ag} by calculating the radius of a sphere with an identical cross-sectional area: $r_{eq} = \sqrt{\frac{A_{ag}}{\pi}}$.

To determine the experimental shape factors for glass beads and spinel crystals, the measured terminal settling velocities were plotted against $((\rho p-\rho f)*g*R^2)/\eta$. The slopes of the linear regression curves corresponded to the unknown Stokes' shape factors.

iii. Hindered Settling

To study hindered settling, suspensions containing glass beads and spinel crystals in particle volume fractions ranging from 0.01 to 0.04 were prepared. The particles were homogeneously dispersed in silicon oil by placing the container on a double barrel roller for approximately ½ hr. The suspension was then transferred to a quartz cuvette and placed in a vacuum desiccator to remove any air bubbles that may have formed during mixing and pouring. The tested particle size distributions, densities and volume concentrations are shown in Table 1.

It was seen that electrostatic forces could accumulate during the rolling and pouring stages, causing particles to stick to the cuvette walls during settling. To prevent charge

accumulation due to particle-particle and particle-wall interactions, anti-static sheets were wrapped around the bottles during mixing and used to cover two walls of the cuvette during settling. A digital camera mounted on a tripod was used to capture the successive images of the settling front. The collected images were analyzed with PAX-it imaging software to obtain the distance of settling front from top oil surface. The velocity of the settling front was calculated by dividing the difference in settling front position between successive images by the known time interval.

Color threshold analysis (CTA) was used to find the upper and lower uncertainties in the settling front position and the concentration profile of particles in the cuvette for each of the images. CTA determined the percentage of voids (gray colored background) showing through the dispersed particles. The concentration profile was determined by dividing the cuvette into a series of equally ~10 rectangles sized rectangles drawn contiguously along its. PAX-it imaging software was used to obtain the percentage of voids in each rectangle. The regions of the cuvette above and below the settling front that showed no significant difference in particle volume fraction were assumed to contain the same void concentration as the highest or lowest measurement, respectively. An example of the analysis is shown in Figure 4. The top of the oil was used as the starting point and the position of each rectangle was taken to be the vertical distance from the top of the oil to the center of the rectangle. Using the concentration profiles, the rate of clarification (increase in the void concentration) at any given rectangle position was found by plotting the void concentration in that rectangle against the time at which the image was taken.

iv. Inclined Settling

In order to measure the increased volumetric settling rate in inclined vessels, the cuvette was placed on stables holders inclined at 60 and 30º with respect to the vertical. The suspension was prepared and photographed as before. Since the cuvettes were inclined, the concentration gradient was found by drawing parallelograms of equal dimensions as those used in the vertical settling CTA.

3. Results and Discussion

i. Shape Factor

To validate our experimental method, the shape factor of single glass beads was measured and compared to the expected value from the Stokes' equation (1). This was done by plotting the measured terminal settling velocity vs. $((\rho p-\rho f)*g*R^2)/\eta$ and calculating the slope (shape factor) of the best fit linear regression line. Figure 5 shows the plots for both glass beads and spinel crystals. The linear regression line for glass beads showed little variance and the calculated shape factor 0.2206 differed only 0.73% compared to the theoretical shape factor 2/9 for a perfect sphere.

The calculated shape factor of octahedral spinel crystals was slightly lower than the glass beads. This can be attributed to larger drag forces caused by a higher surface area to volume ratio. Spheres have the smallest surface area for all shapes of a given volume and at low Reynolds numbers experience a minimum amount of resistance as they travel through a fluid. A decrease in the sphericity, corresponding to an increase in the surface area to volume ratio, results in an increase in the surface drag and a decrease in velocity for an object travelling through a given fluid. Authors Happel and Brenner used a Stokes' shape factor correlated to the particle sphericity through the equation [5]:

$$k' = 0.843 \times \log_{10} \frac{\psi}{0.065} \qquad (5)$$

where the sphericity ψ is defined as the ratio of the surface area of a sphere to the surface area of a particle with the same volume. If multiplied by 2/9, this shape factor becomes the Stokes' shape factor *k* from equation (2). Table 2 compares the experimentally determined shape factors for glass beads and spinel crystals with the corresponding theoretical shape factors calculated from equation (5). The spinel shape factor of 0.1896 differed by 9.2% compared to the theoretical Stoke's shape factor of 0.2087. This difference can be attributed to the higher scatter of data (smaller R^2 value) resulting from irregularities in crystal shape (e.g., crystal elongation shown in Figure 1), surface defects, and differences in crystal orientation during settling. Variations in crystal geometry cause a divergence from the sphericity of an isometric octahedron. The effects of these parameters on the spinel shape factor could not be quantified in the shallow three-dimensional images collected during the settling experiments.

The data in Figure 5 show that the calculated shape factors for spinel agglomerates were widely scattered. Case to case variations in the number of agglomerated crystals, the degree of overlap, and the agglomerate orientation can explain this variance. In addition, multi-particle agglomerates likely contained holes or inter-pockets that slowed their settling velocity. This is supported by the fact that when only two- or three-particle agglomerates were considered, the determined shape factor was 0.1847 – almost identical to that of the single spinel crystals. Unfortunately, these features could not be distinguished in the shallow three-dimensional images. To better predict the settling velocity of complex agglomerates, a new experimental technique with greater sensitivity to these features needs to be developed.

ii. Hindered Settling

The motion of the hindered settling front in high particle volume fraction suspensions of glass beads and spinel crystals was used to study the behavior of spinel crystals in glass melts containing a high volume fraction of crystals. To discriminate between the regions formed by particle separation, three distinct regions of the suspension were defined: 1) the clarified fluid at the top of the settling vessel, 2) the transition region where the concentration varied from nearly clarified to more concentrated, and 3) the region of the suspension containing all particle sizes in nearly their original concentrations. The settling front position was defined to be somewhere in the transition region, but particle diffusion and polydispersity made the accurate determination of a position difficult, particularly in low-viscosity and low-concentration suspensions.

To account for particle separation, the extension of the transition region was used as a measure of settling front position uncertainty. For glass beads, an initial settling front position was presumed near the center of the transition region and then the distances (uncertainties) upward to clarified fluid and downward to the original concentration were measured. This position was corrected by subtracting the upper uncertainty from the initial measurement and then adding half of the total transition region extension. This situated the settling front position in the middle of the transition region with equal uncertainties above and below. Typical examples of settling front movement and the associated uncertainties are shown in Figure 6 and the comparison of settling velocity vs. hindered settling function for all tested cases is given in Figure 7. The wider size distribution of spinel crystals (149-212 μm) compared to glass beads (150-180 μm) led to a broader transition region and a correspondingly greater degree of difficulty in locating an initial settling front position. Therefore, a determined volume fraction, corresponding to a specific crystal size, was used to define the position of the settling front and

CTA was used to verify that the volume fraction of crystals around this point was fairly constant. Table 3 shows the variations in the percentage of voids above and below the settling front during the hindered settling of spinel crystals. Two important limitations in the accuracy of CTA to determine void concentrations were the clarity of images and the size of particles. Larger particles produced the high contrast images that were evaluated with high precision using CTA. The lack of contrast in slightly blurred images and images containing smaller particles complicated the CTA because the distributions of white and black points for the edge of particles were not that different from the background. In addition, small variations in lighting between the successive images also complicated the CTA.

The apparent particle sizes, or the monodisperse particle sizes with the same settling front velocity as that measured, consistently corresponded to the particle sizes at the lower end of the size distribution. These were found by solving (3) for *u* and then substituting this value into (1) and solving for *r*. Table 4 shows how the apparent particle size varied with volume fraction. The decreasing particle size at higher particle volume fractions can be explained by the number of particles in the suspension. At lower volume fractions, the concentration of small beads was low. However, at higher volume fractions, the smaller beads were more numerous and were detected by color threshold analysis. The apparent particle size of the spinel did not vary significantly because a specific volume fraction of crystals of about the same size was followed in the images.

Figure 8 shows the concentration gradient development for the 1 vol% spinel suspension. Initially, the entire cuvette contained 1 vol% of homogeneously dispersed spinel crystals, with the exception of a small area close to the top surface where crystal settling was immediately visible. However, toward the end of the experiment, there was a continuous increase in crystal concentration from top to bottom over nearly the entire length of the cuvette. This can be

explained by the different settling velocities of the polydisperse spinel crystals. The gradient lines of glass beads were significantly steeper, as can be seen in Figure 9, indicating a much more well-defined settling front. The concentration profiles were compared to the measured settling front velocities by plotting the average void concentration obtained from the settling front uncertainty measurements and finding the points where this concentration crossed each individual concentration gradient line. Using the known times corresponding to each gradient line and the distances between gradient lines, the settling velocities were found and compared to the velocities from the direct settling front measurements. This comparison is summarized in Table 3.

Figure 10 shows how the void concentration in suspensions of different crystal volume concentrations changed with time at a point about 4.5mm from the top of the oil. The 0.5 and 1.0 vol% spinel crystal solutions clarified at nearly identical rates except for a small difference in void concentration at the beginning of the settling experiment. In contrast, the void concentration of the 1.5 vol% suspension started out much lower and then increased more rapidly compared to 0.5 and 1.0 vol% suspensions. This was unexpected given the decreased velocities for the higher volume fraction suspensions that were calculated from the Richardson-Zaki equation. The increased rate of clarification in the 1.5 vol% suspension could be due to the larger number of bigger particles causing the solution to appear more clarified once they had passed.

iii. Inclined Settling

In the inclined settling experiments, the concentration of spinel crystals decreased more rapidly than in the vertical settling experiments and the rate of clarification increased with increasing angle from the vertical. Figure 11 shows that the concentration of voids approximately 4.5 mm from the surface increased more rapidly at cuvette angles of 60º than 30º. Figure 12

details the concentration gradient of voids along the length of the incline and vertical cuvettes after 23 minutes. Particle suspensions in both inclined cuvettes are more clarified than the vertical cuvette containing the same volume fraction of particles. This suggests that any incline of the spout riser plays an important role in an accurate prediction of spinel settling in the HLW glass melters.

4. Conclusion

The free settling experiments with spherical glass beads produced a Stokes' shape factor very close to the predicted theoretical value. This provided confidence in the experimental setup and confirmed the appropriate use of developed methodology to study free settling of single particles. The experimental shape factor for the spinel crystals was smaller than that of the beads due to the higher surface drag caused by the larger surface area to volume ratio of the octahedral crystals and was about 10% lower compared to the non-spherical shape factor calculated from equation used by Happel and Brenner. The concentrated suspensions of glass beads and spinel separated into distinct regions of varying concentration due to polydispersity and hindered settling effects. The settling front was defined as the middle of the transition region and the uncertainty of its position increased with time. As predicted by the Richardson-Zaki equation, the settling front velocity decreased as the volume fraction of the suspension increased. Also, the average particle size decreased at higher volume fractions due to increased number of smaller particles detected by CTA. The particle concentration profiles identified a large degree of separation in the spinel settling experiments due to wide size distribution of spinel crystals (149-212 μm). The two methods used to find the settling front velocity – direct measurement from the images and plotting the concentration profiles – yielded similar results, though the variance in the second method was several times that of the first. This provided confidence that CTA

produced reliable values for relative concentration and that the settling front measurements followed a steady concentration. The unexpected result that higher particle volume fractions clarified at a faster rate could be explained by the number of larger particles in the suspension. The larger particles would settle out more quickly and thus a larger percentage of voids would be detected by CTA. Settling of crystals in inclined cuvettes proceeded more rapidly than vertical cuvettes containing the same volume fraction and was faster for higher angles with respect to the vertical. The physical modeling of free and hindered settling of particles is a useful tool to study the settling behavior of spinel crystals in the high viscosity liquids. The Stokes' and Richardson-Zaki equations can adequately predict the accumulation rate of spinel crystals in the glass discharge riser of HLW melters.

5. Acknowledgements

The authors would like to thank Mike Schweiger for laboratory support, Carol Burnett for supplying materials, and Brian Riley for technical support. Micah would like to thank the Office of Science for his internship opportunity at Pacific Northwest National Laboratory (PNNL), which is operated for the U.S. Department of Energy (DOE) by Battelle under Contract DE-AC06-76RLO 1830. All of the research performed in this paper was done in the Applied Processes and Engineering Laboratory at PNNL during Micah's internship appointment in Spring/Summer 2009. The research was funded by DOE Environmental Management Program.

6. References

1. P. Hrma, P. Schill, L. Nemec, "Settling of Spinel in a High-Level Waste Glass Melter", US Department of Energy Final Report, 2001

2. P. R. Hrma, "Impact of Particle Size and Agglomeration on Settling of Solids in Continuous Melters Processing Radioactive Waste Glass", *Journal of Nuclear Materials,* December 2008

3. J. Happel, H. Brenner, *Low Reynolds Number Hydrodynamics: with special applications to particulate media.* The Hague ; Boston : M. Nijhoff ; Hingham, MA, USA : Distributed by Kluwer Boston, 1983, pp. 411

4. *Ibid.* pp.219

5. R. P. Chhabra, L. Agarwal, N. K. Sinha, "Drag on non-spherical particle: an evaluation of the available methods," *Powder Technology*, vol. 101, pp. 288-295, 1999

6. A. Hazzab, A. Terfous, A. Ghenaim, "Measurement and modeling of the settling velocity of isometric particles," *Powder Technology*, vol. 184, pp. 105-113, 2008

7. R. H. Davis, A. Acrivos, "Sedimentation of Non-Colloidal Particles at Low Reynolds Numbers," *Annual Review of Fluid Mechanics*, vol. 17, pp. 91-118, 1985

8. P. Izak, P. Hrma, B. W. Arey, T. J. Plaisted, "Effect of feed melting, temperature history, and minor component addition on spinel crystallization in high-level waste glass," *Journal of Non-Crystalline Solids*, vol. 289, pp. 17-29, 2001

9. J. Alton, T.J. Plaisted, P. Hrma, "Dissolution and growth of spinel crystals in a borosilicate glass," *Journal of Non-Crystalline Solids*, vol. 311, pp. 24-35, 2002

10. J. Alton, T. J. Plaisted, P. Hrma, "Kinetics of growth of spinel crystals in a borosilicate glass," *Chemical Engineering Science*, vol. 57 (13), pp. 2503-2509, 2002

11. S. Lee, Y. Jang, C. Choi, T. Lee, "Combined effect of sedimentation velocity fluctuation and self-sharpening on interface broadening," *Physics of Fluids A*, vol. 4 (12), 1992

12. R. A. Williams, C. G. Xie, R Bragg, W. P. K. Amarasinghe, "Experimental Techniques for Monitoring Sedimentation in Optically Opaque Suspensions," *Colloids and Surfaces*, vol. 43, pp. 1-13, 1990

13. E. Doroodchi, D. F. Fletcher, K. P. Galvin, "Influence of inclined plates on the expansion behavior of particulate suspensions in a liquid fluidized bed," *Chemical Engineering Science*, vol. 59, pp. 3559-3567, 2004

7. Appendix

i. Figures

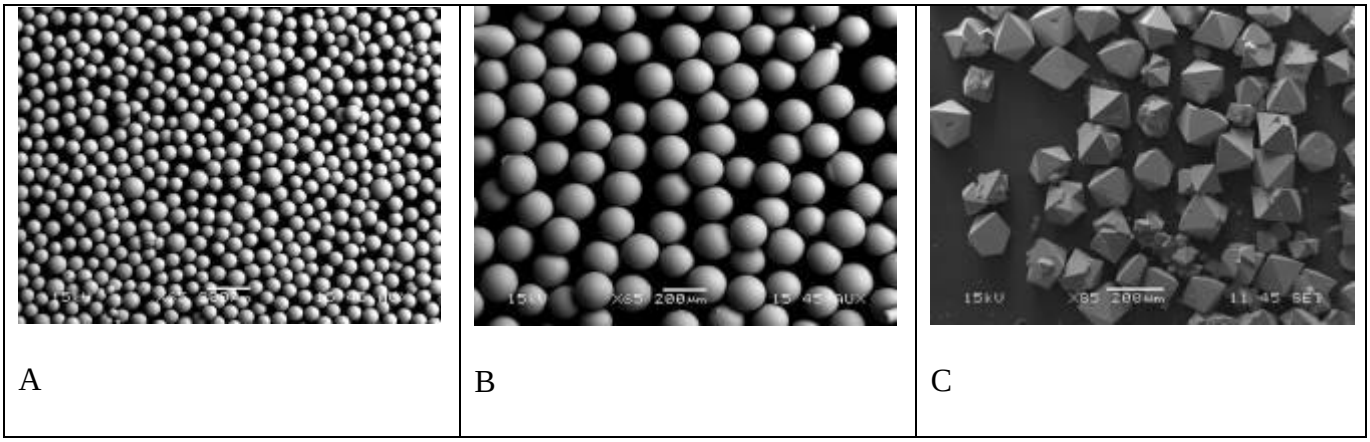

A B C

Figure 1: SEM images of barium calcium silicate glass beads; 70-80 µm (A), 150-180 µm (B); and spinel crystals isolated from the waste glass simulant; 100-149 µm (C).

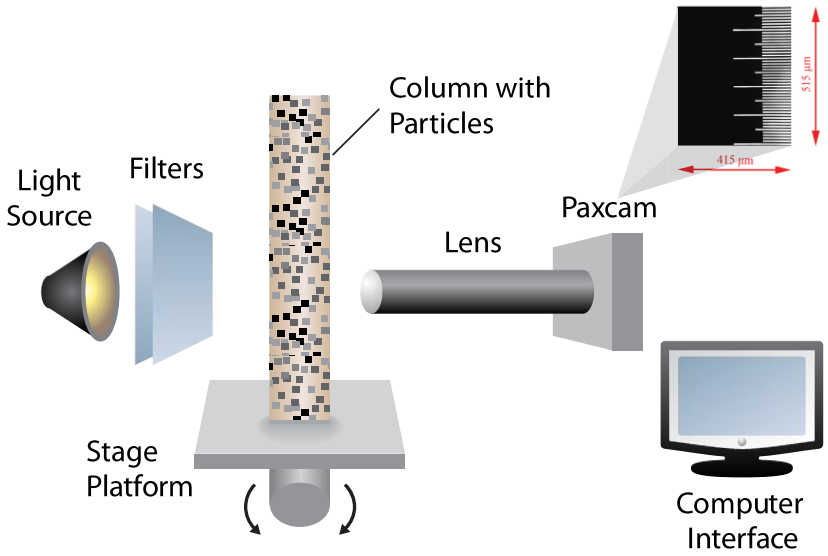

Figure 2: Optical particle-dynamics-analyzer configuration for measurement of the free settling velocity of individual glass beads and spinel crystals.

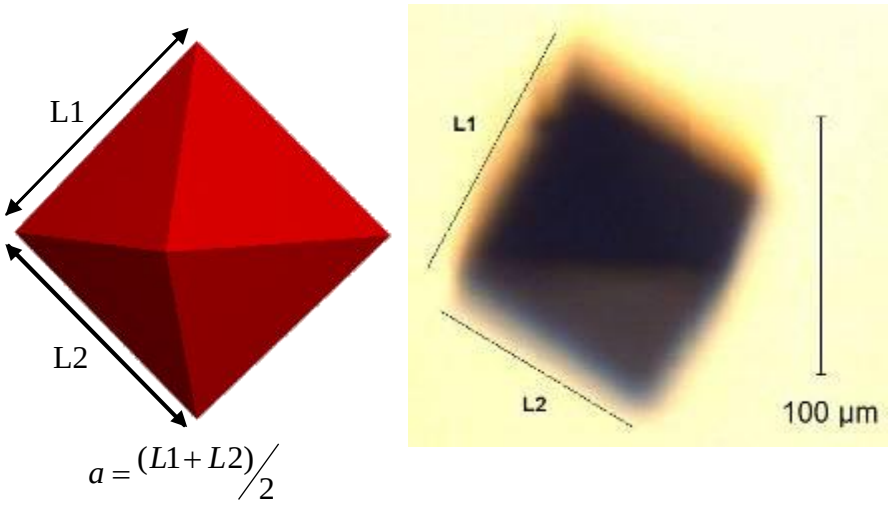

Figure 3: Picture of isomeric octahedron and shallow three-dimensional optical image of captured spinel crystal with measured edge lengths. Variations in crystal shape and surface defects cannot be clearly identified in these images.

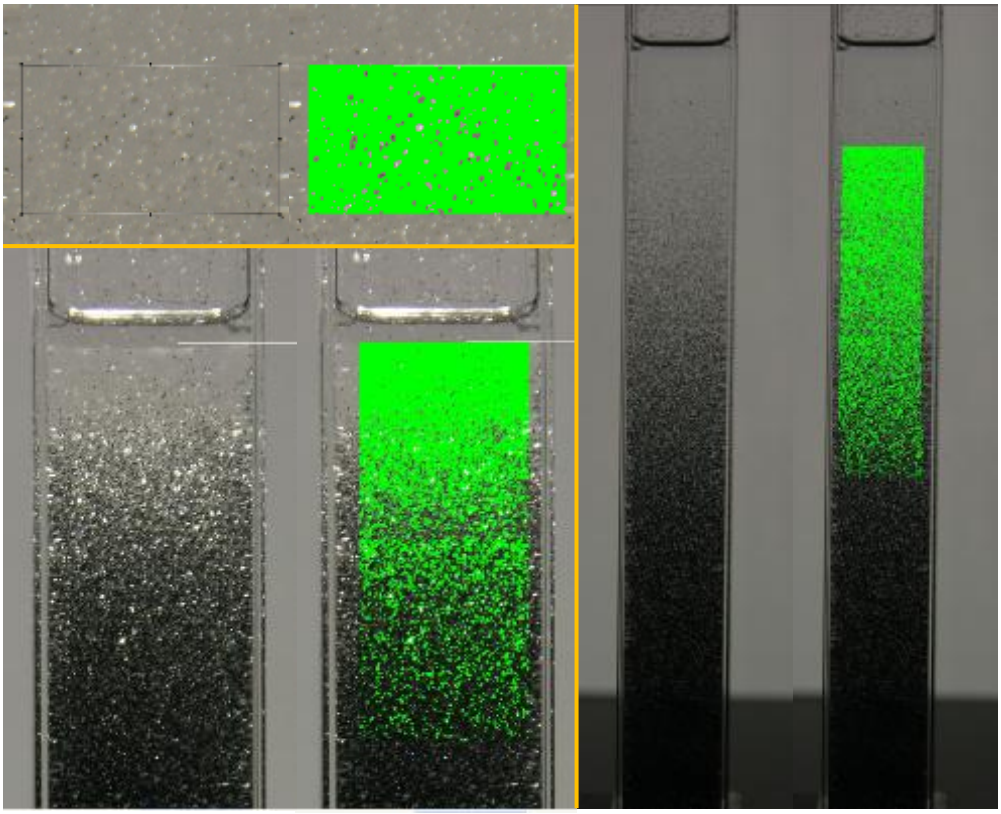

Figure 4: Example of Color Threshold Analysis (CTA) that was used to determine the percentage of voids in particle suspensions of different concentrations and to compare the relative concentration to measured settling front velocity.

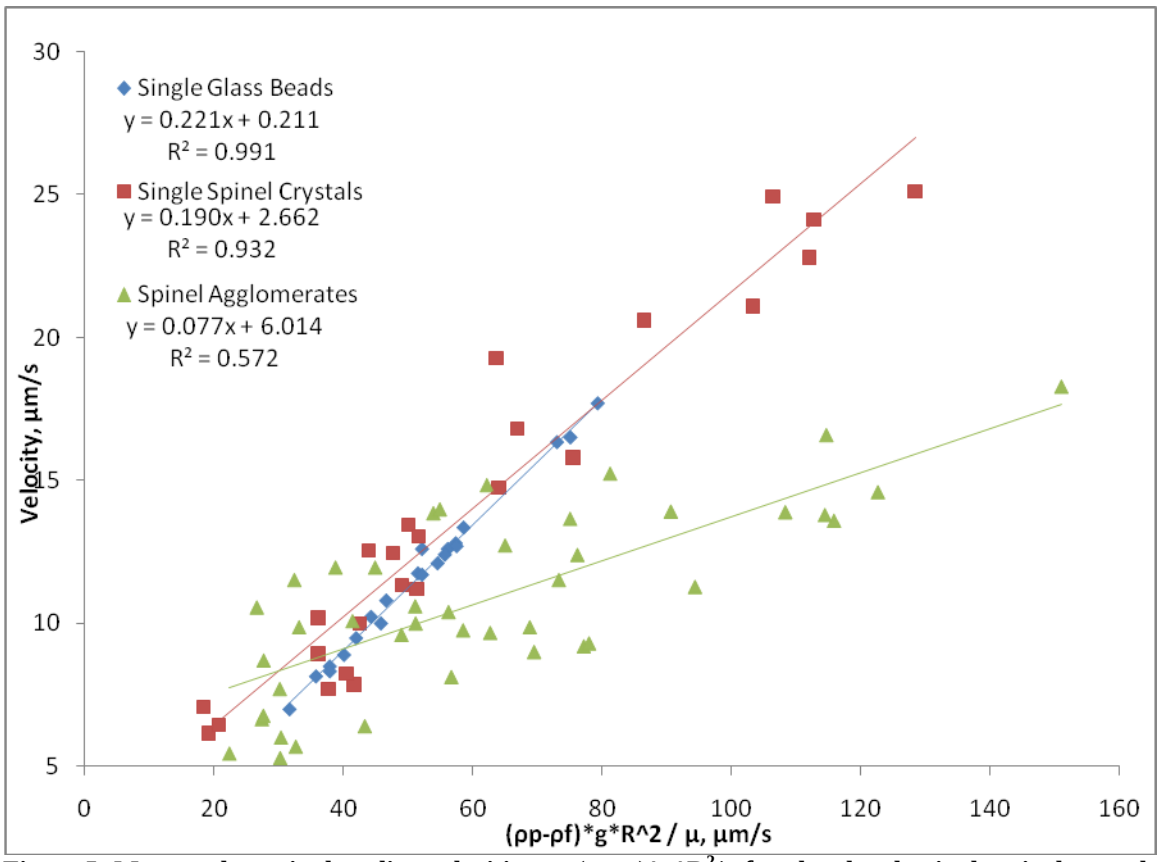

Figure 5: Measured terminal settling velocities vs. $(\rho_p-\rho_f)*g*R^2/\mu$ for glass beads, single spinel crystals and spinel agglomerates. The slopes of fitted lines correspond to experimentally determined shape factors.

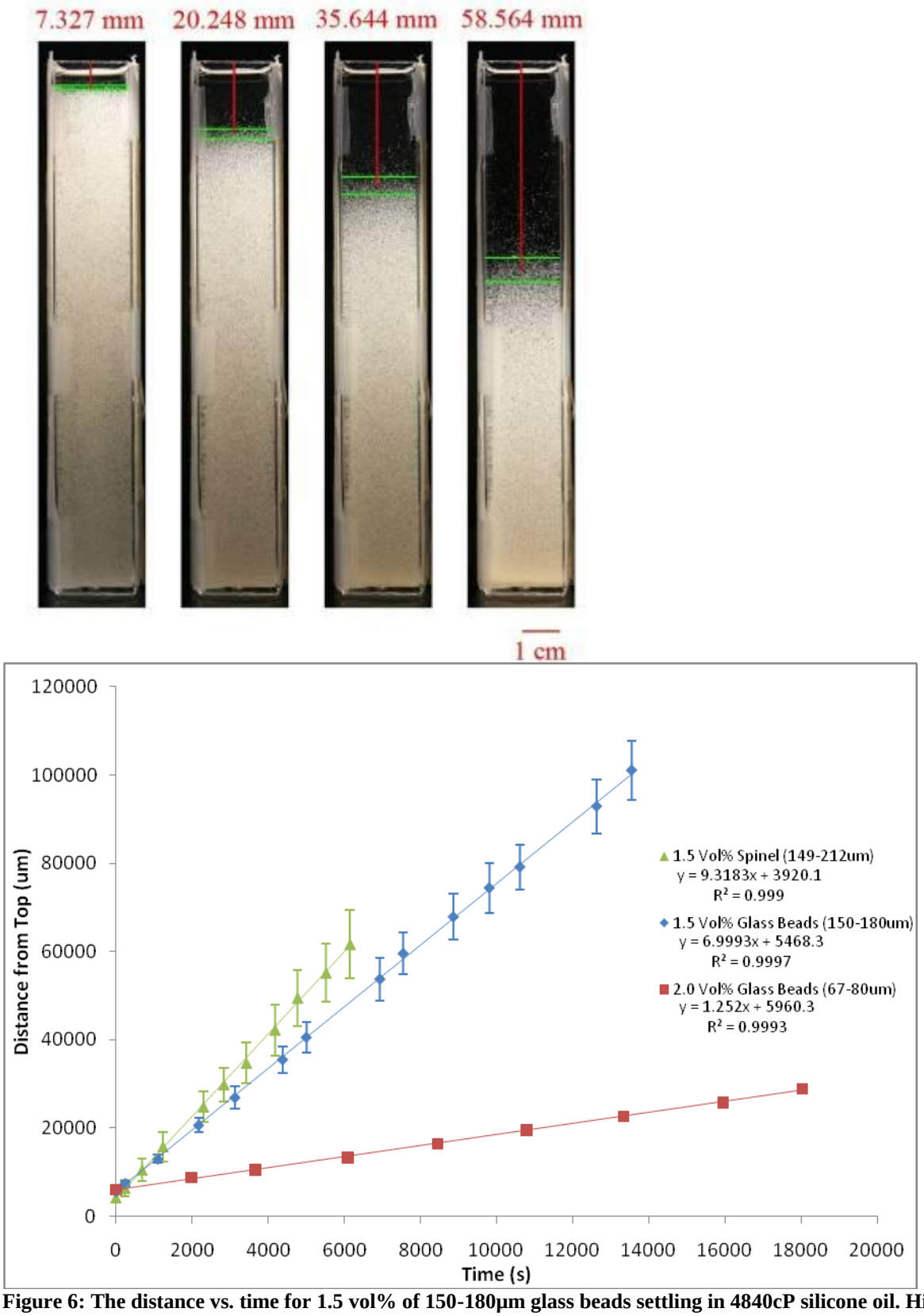

Figure 6: The distance vs. time for 1.5 vol% of 150-180µm glass beads settling in 4840cP silicone oil. Hindered settling velocity is dependent primarily on particle size and secondarily on particle shape. The uncertainty in settling front position (the error bars) increases with time.

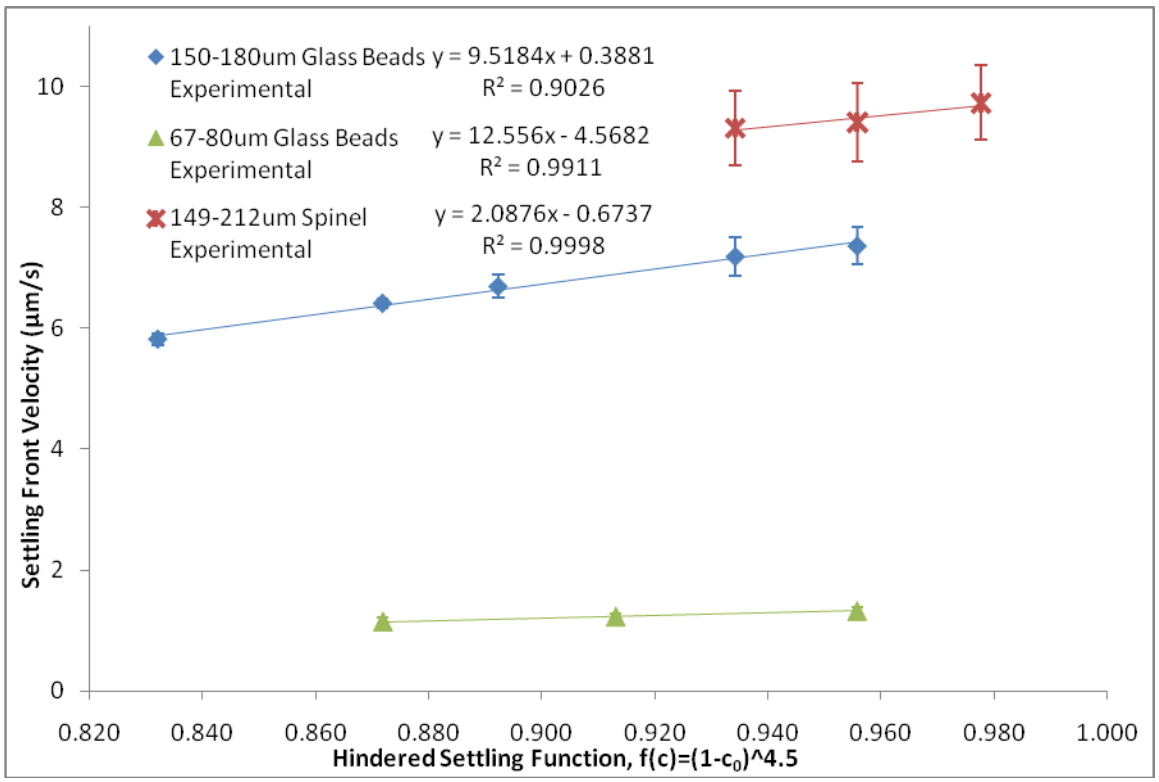

Figure 7: Settling front velocity vs. hindered settling function for two sizes of glass beads and spinel crystals. The narrower particle size distribution corresponds to lower uncertainty of measurement.

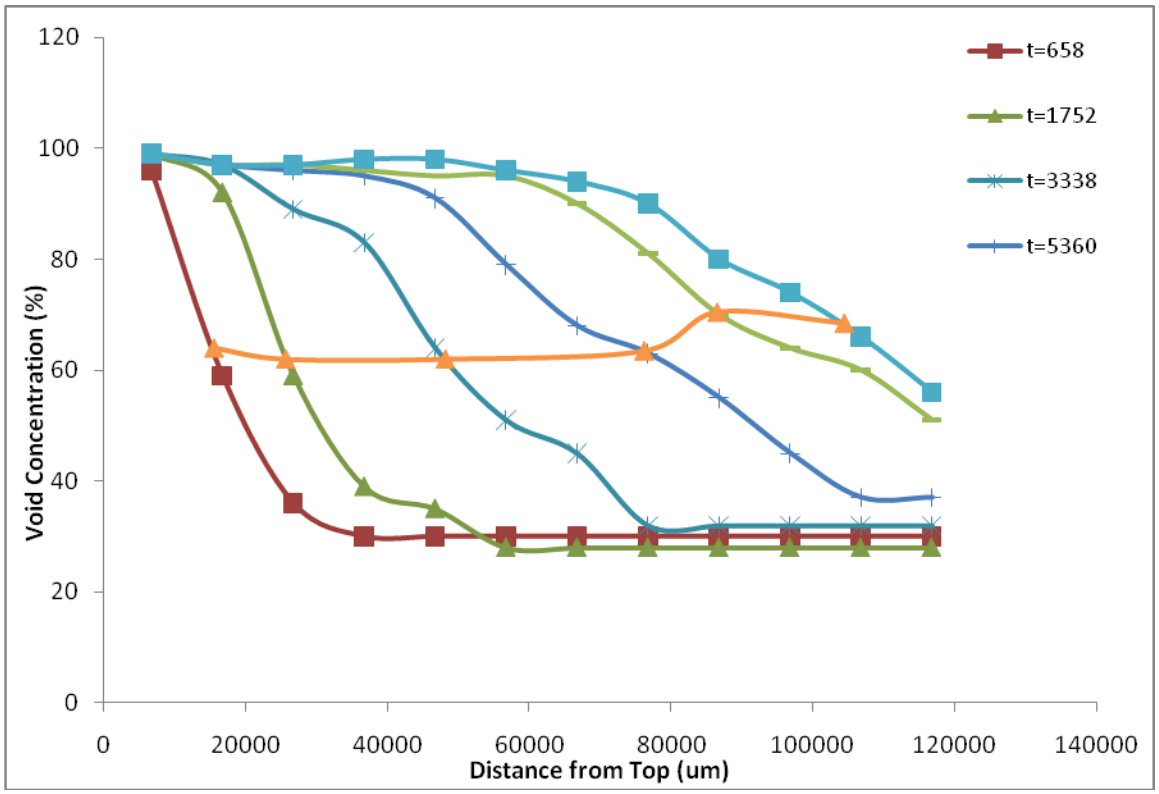

Figure 8: Concentration gradient of voids over the length of the cuvette in successive images for 1.0 vol% spinel suspension. Each line represents a single image of cuvette with spinel crystal suspension.

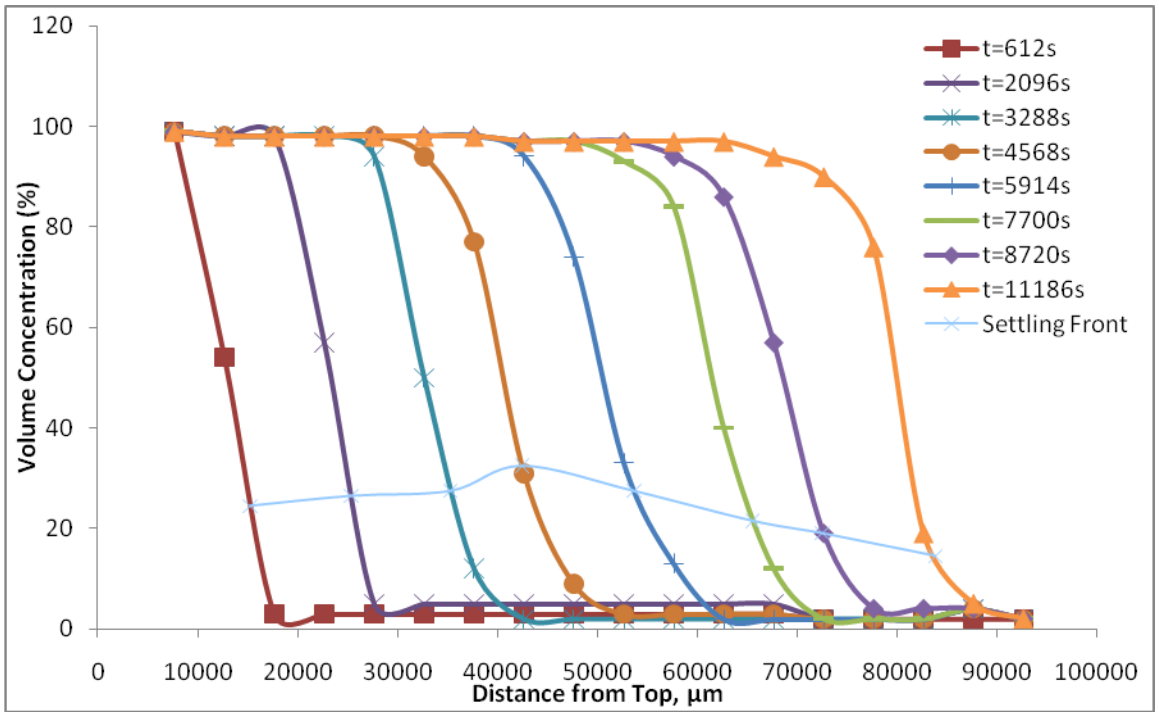

Figure 9: Concentration gradient of voids for 0.5vol% glass beads suspension.

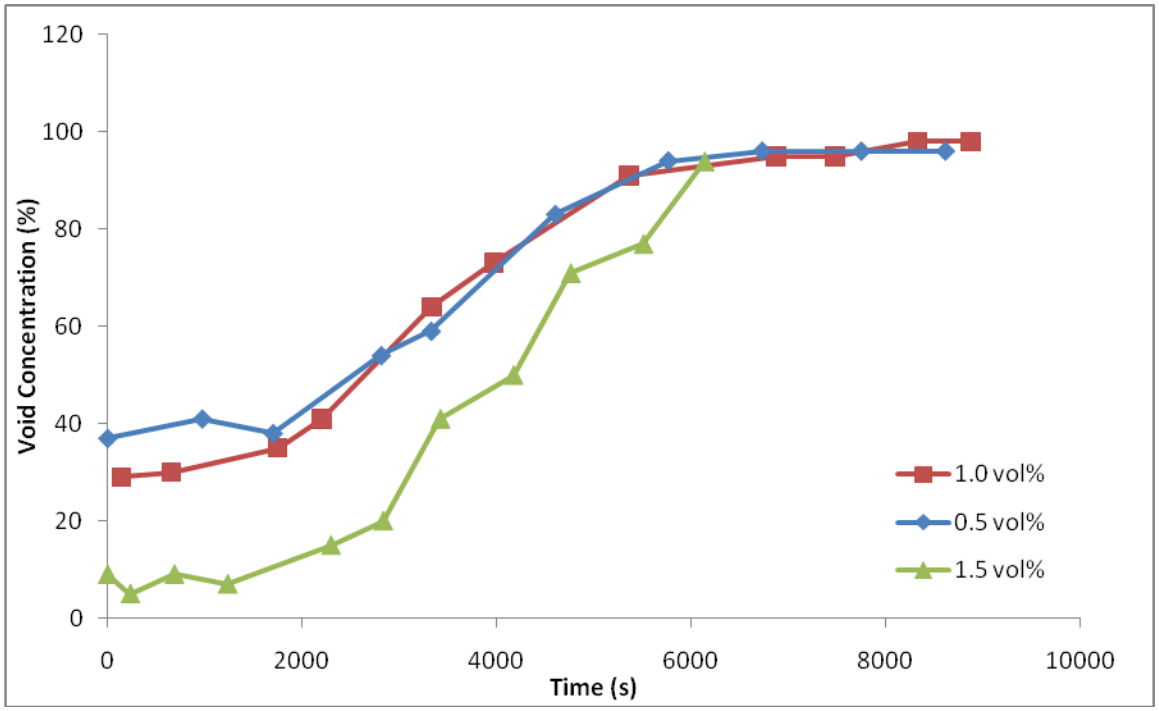

Figure 10: Concentration gradient of voids in different volume fraction suspensions of spinel at ~4.5mm from the top of the oil. The 0.5 and 1.0 vol% suspensions clarified at nearly the same rate while the 1.5 vol % suspension clarified a bit faster after the latent period of 3000s but took longer to reach +90% void concentration.

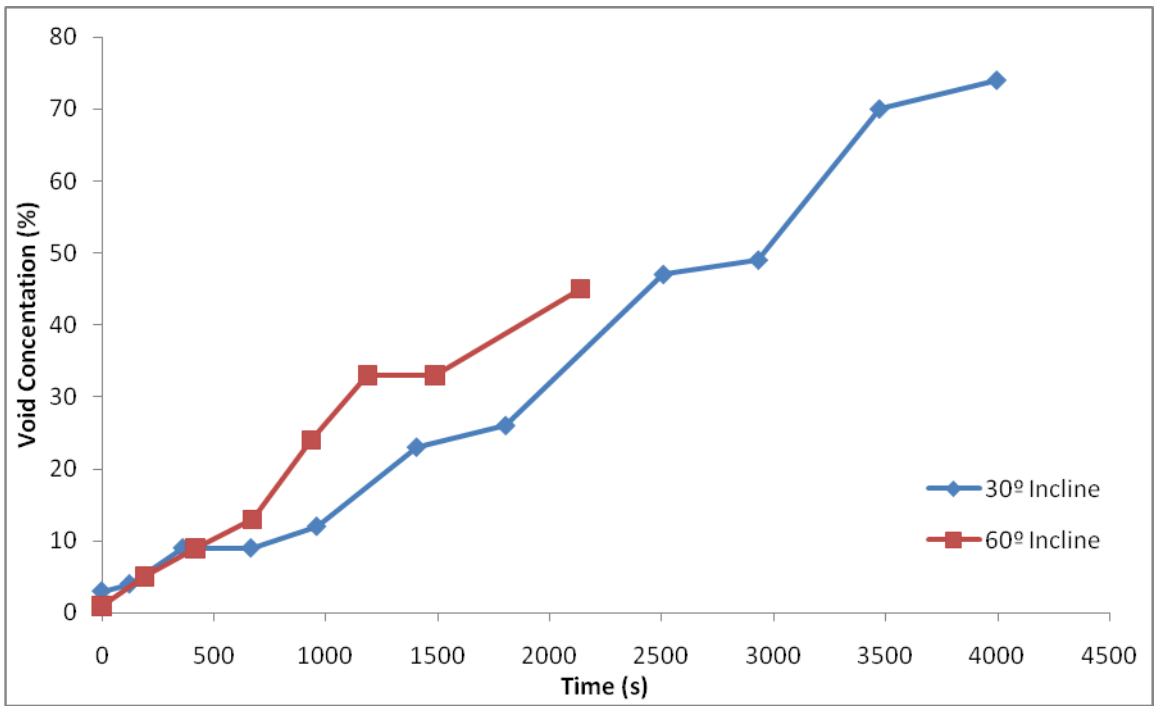

Figure 11: Concentration gradient of voids vs. time for 2.75 vol% suspension in incline cuvettes. A greater angle measured with respect to the vertical corresponds to a higher rate of increase in the void concentration along the length of the cuvette.

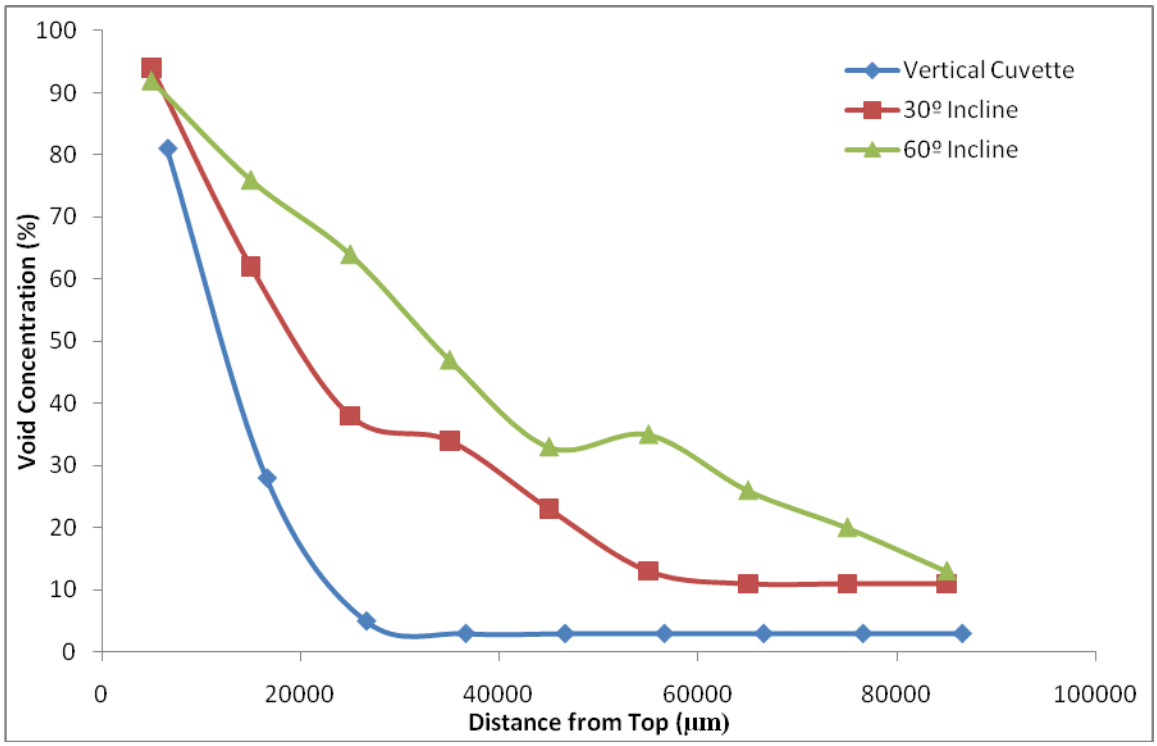

Figure 12: Concentration gradient of voids vs. time for 2.75 vol% suspension in vertical and incline cuvettes. The greater the incline of the settling vessel with respect to the vertical, the more rapid the clarification of the suspension along the length of the cuvette.

ii. Tables

Table 1: Characteristics of particles, silicon oil, and suspensions used in the hindered settling experiments.

Particle size distribution (μm)	Particle density (g/cm^3)	Viscosities of silicone oils (cP)	Calculated Re number for median particle size	Concentration of suspensions (vol%)
Glass beads				
150-180	4.1741	4840	1.62E-07	1.0, 1.5, 2.5, 3.0, 4.0
67-80	4.1741	" "	1.41E-08	1.0. 2.0, 3.0
Spinel				
149-212	5.3954	5080	1.90E-07	0.5, 1.0, 1.5

Table 2: Comparison of experimentally determined shape factors for glass beads and spinel crystals with the non-spherical shape factors calculated from equation (4) used by Happel and Brenner.

	Sphericity	Experimental shape factor	Theoretical shape factor	Percent error
Beads	1	0.2206	0.2222	0.730
Spinel	0.846	0.1896	0.2087	9.168

Table 3: Concentration of voids and settling front velocities for different concentrations of spinel crystal suspensions. Voids were present in higher percentages in lower concentration suspensions and the accuracy in the measured settling front velocity increased at higher concentrations. The settling front velocity found from the concentration profiles is not as accurate, but shows good agreement with the measured. Each value is the average ± 1 standard deviation of at least 10 independent measurements.

Concentration of spinel (vol%)	Concentration of voids above settling front (vol%)	Concentration of voids below settling front (vol%)	Settling front velocity measured from images (μm/s)	Settling front velocity found from concentration profiles (μm/s)
0.50	79.55 ± 3.297	73.27 ± 8.223	9.73 ± 0.97	9.30 ± 2.22
1.00	69.25 ± 3.720	61.25 ± 5.754	9.41 ± 0.80	10.36 ± 4.15
1.50	64.09 ± 4.805	57.09 ± 6.949	9.32 ± 0.42	9.69 ± 5.23

Table 4: Experimentally measured settling front velocities and calculated apparent particle sizes from the hindered settling experiments.

Concentration of particles (vol%)	Experimentally measured settling front velocities for 150-180μm glass beads (μm/s)	Calculated bead size for 150-180μm glass beads (μm)	Experimentally measured settling front velocities for 67-80μm glass beads (μm/s)	Calculated bead size for 67-80μm (μm)	Experimentally measured settling front velocity for 149-212μm spinel (um/s)	Calculated spinel crystal size (μm)
0.5%	---	---	---	---	9.733	166.2
1.0%	7.368	146.2	1.322	61.9	9.407	165.3
1.5%	7.192	146.1	---	---	9.320	166.5
2.0%	---	---	1.231	61.1	---	---
2.5%	6.696	144.2	---	---	---	---
3.0%	6.417	142.8	1.147	60.4	---	---
4.0%	5.820	139.2	---	---	---	---